G. Grégoire, Z. Janout, K. Kuroda, A. Michalowicz, M. Poulet, D. Sillou, G. Bellettini, P. L. Braccini, T. del Prete, L. Foa, P. Laurelli, G. Sanguinetti, and M. Valdata, Phys. Lett. **36B**, 493 (1971).
[11]M. G. Albrow, S. Andersson/Almehed, B. Bošnjaković, C. Daum, F. C. Erné, J. P. Lagnaux, J. C. Sens, and F. Udo, Nucl. Phys. **B25**, 9 (1970).
[12]M. G. Albrow, S. Andersson/Almehed, B. Bošnjaković, C. Daum, F. C. Erné, Y. Kimura, J. P. Lagnaux, J. C. Sens, and F. Udo, Nucl. Phys. **B37**, 594 (1972).
[13]G. Burleson, D. Hill, S. Kato, P. F. M. Koehler, T. B. Novey, A. Yokosawa, D. Eartly, K. Pretzl, B. Ba.. ·tt, A. Laasanen, and P. Steinberg, Phys. Rev. Lett. **26**, 338 (1971).
[14]A. Citron, W. Galbraith, T. F. Kycia, B. A. Leontič, R. H. Phillips, A. Rousset, and P. H. Sharp, Phys. Rev. **144**, 1101 (1966); A. A. Carter *et al.*, Phys. Rev. **168**, 1457 (1968).
[15]R. J. N. Phillips and W. Rarita, Phys. Rev. **139**, B1336 (1965); C. B. Chiu, R. J. N. Phillips and W. Rarita, Phys. Rev. **153**, 1485 (1967); C. B. Chiu, S. Chu and L. Wang, Phys. Rev. **161**, 1563 (1967); W. Rarita, R. J. Riddell, C. B. Chiu and R. J. N. Phillips, Phys. Rev. **165**, 1615 (1968); V. Barger and R. J. N. Phillips, Phys. Rev. Lett. **20**, 546 (1968); Phys. Rev. Lett. **22**, 116 (1969); Phys. Lett. **29B**, 503 (1969); A. Beretvas and N. E. Booth, Phys. Rev. Lett. **22**, 113 (1969).
[16]V. Barger and R. J. N. Phillips, Phys. Rev. **187**, 2210 (1969).
[17]J. A. Scheid, doctoral dissertation, Department of Physics, University of Chicago (unpublished).
[18]The sign of the target polarization is defined as positive when parallel to the vector $\vec{k}_i \times \vec{k}_f$, where $\vec{k}_i$ and $\vec{k}_f$ are the initial and final momenta of the pion.
[19]V. Singh, Phys. Rev. **129**, 1889 (1963).
[20]N. E. Booth, Rutherford Laboratory Report No. RPP/H/58, 1969 (unpublished).
[21]O. Guisan, in *Proceedings of the Second International Conference on Polarized Targets*, edited by G. Shapiro (Univ. of Calif. Press, Berkeley, Calif., 1971), p. 187; more recent results from Argonne however do not indicate such large values of P_x [D. Hill *et al.*, Phys. Rev. Lett. 28, 239 (1973)].
[22]P. Bonamy *et al.*, Nucl. Phys. **B16**, 335 (1970); D. Drobnis *et al.*, Phys. Rev. Lett. **20**, 274 (1968).
[23]G. Conforto, in *High Energy Collisions*, edited by C. N. Yang *et al.* (Gordon and Breach, New York, 1969) p. 51.
[24]F. Halzen and C. Michael, Phys. Lett. **36B**, 367 (1971); R. L. Kelly, Phys. Lett. 39B, 635 (1972).
[25]V. Barger and F. Halzen, Phys. Rev. Lett. **30**, 194 (1972).

PHYSICAL REVIEW D VOLUME 8, NUMBER 5 1 SEPTEMBER 1973

Total and Partial γp Cross Sections at 9.3 GeV*

H. H. Bingham, W. B. Fretter, W. J. Podolsky,† M. S. Rabin,‡ A. H. Rosenfeld, and G. Smadja§
University of California and Lawrence Berkeley Laboratory, Berkeley, California 94720

J. Ballam, G. B. Chadwick, Y. Eisenberg,‖ R. Gearhart, E. Kogan,‖ K. C. Moffeit, J. J. Murray, P. Seyboth,** C. K. Sinclair, I. O. Skillicorn,†† H. Spitzer,‡‡ and G. Wolf§§
Stanford Linear Accelerator Center, Stanford University, Stanford, California 94305

(Received 12 March 1973)

We report γp total, topological, and channel cross sections at 9.3 GeV from a bubble-chamber experiment using a nearly monoenergetic photon beam.

I. INTRODUCTION

In this paper we report photoproduction cross sections obtained by exposing the SLAC-LBL 82-in. hydrogen bubble chamber to the 9.3-GeV SLAC backscattered laser beam. The experimental procedures are similar to those of our previous experiments at 2.8 and 4.7 GeV.[1] The photon beam has an energy spread of 6.4% [full width at half maximum (FWHM)].

We obtain the total hadronic γp cross section, topological cross sections for charged multiplicities of 1 to 9, and channel cross sections for the following channels:

$$\left.\begin{aligned} &\gamma p \to p + m\pi^+ + m\pi^- \\ &\gamma p \to p + m\pi^+ + m\pi^- + \pi^0 \\ &\gamma p \to n + (m+1)\,\pi^+ + m\pi^- \end{aligned}\right\} m = 1, 2, 3, 4$$

$$\gamma p \to p + K^+ + K^- + l\pi^+ + l\pi^-, \quad l = 0, 1, 2$$

$$\gamma p \to 2p + \bar{p}\ .$$

In Sec. II we describe the beam and event analysis. In Sec. III the procedures for obtaining cross sections are described. Results are reported and discussed in Sec. IV.

II. EXPERIMENTAL PROCEDURE

A. Photon Beam

The beam used in this experiment was similar to that used in our lower-energy experiment and has been described in detail in Refs. 2 and 3. To obtain backscattered photons with energies >6.5 GeV at present SLAC electron beam energies, the linearly polarized red light from a Q-switched ruby laser had to be frequency doubled. We used a KDP (potassium dihydrogen phosphate) or ADP

(ammonium dihydrogen phosphate) crystal and achieved an energy conversion efficiency of ~20%. The resulting linearly polarized blue light (photon energy of 3.56 eV and a total power of ~0.6 joule per pulse) was backscattered from a 19-GeV electron beam of 4×10^{11} electrons per pulse. About 50 high-energy photons per pulse were obtained in the bubble chamber. Figure 1 shows the photon spectrum. The average energy is 9.3 GeV and the FWHM is 0.6 GeV. The low-energy tail of the spectrum ($0.5 \leq E_\gamma \leq 8$ GeV) contains 7.6% of the photons. The degree of linear polarization of the backscattered photon beam was calculated using the formalism of Ref. 4 by averaging over the experimental energy spectrum between 8 and 10.3 GeV, and by assuming 100% linear polarization for the incident blue light. The resulting linear polarization was found to be 77%.

A total of 1 260 000 pictures were taken in four exposures differing slightly in energy. To minimize possible biases the polarization of the photons in the bubble chamber was rotated by 90° for about half of the experiment. Table I gives a summary of the beam parameters and exposure statistics.

B. Event Analysis

All pictures were double-scanned as described in Refs. 1 and 3. Pairs were counted in both scans on every 100th frame. Both laboratories scanned

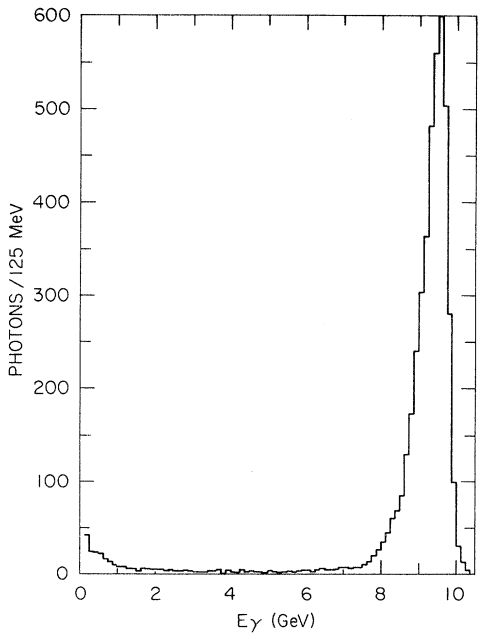

FIG. 1. Photon energy spectrum (unnormalized) in this experiment. For details of calculation see Sec. III A. The spectra of the different exposures have been shifted to their over-all average of 9.3 GeV.

TABLE I. Beam parameters and exposure statistics.[a]

Exposure	Average beam energy, E_γ (GeV)	No. of pictures	Photon polarization in BC[b]
1	9.22	410 000	horiz.
2	9.47	240 000	vert.
3	9.34	320 000	vert.
4	9.23	290 000	horiz.
Sum		1 260 000	

[a] For all exposures: FWHM = 0.6 GeV; E_γ limits accepted = 8–10.3 GeV; average linear polarization P_γ = 77%; events/μb in E_γ limits = 289 ± 6.

[b] Vertical = photon electric vector parallel to optical axis of bubble chamber.

a common subset of the film (10%). A comparison of these scan results for the two laboratories was used to obtain scanning efficiencies. The uncorrected numbers of events found in the scan are given in Table II.

All first measurements were made on the Spiral Reader II at LBL. Remeasurements were done on conventional machines at LBL and SLAC. When remeasurements were stopped, about 1% of the events remained to be remeasured. Depending on the topology, between 5% and 10% of the events could not be measured due to secondary interactions. The geometrical and kinematical reconstruction was done as in Ref. 1, using the kinematic hypotheses listed above in Sec. I.

After completion of the event analysis, one-half of the events were carefully checked for systematic errors in processing. It was found that in fewer than 1% of the events an e^+e^- pair track had been measured instead of the correct hadronic track. Also, in fewer than 1% of the events a proton had been misidentified as a pion or vice versa. By reprocessing these events the systematic errors were further reduced.

The reconstruction procedure was checked by measuring K^0 decays. The $\pi^+\pi^-$ mass distribution of such decays, calculated from the measured track quantities, yielded $M_{K^0} = 498.44 \pm 0.15$ MeV, indicating that the magnetic field was correct to within 0.25%. The measured width of the K^0 peak is ±4.5 MeV [two-constraint (2C) fits], in agreement with the calculated mass resolution.

III. DETERMINATION OF CROSS SECTIONS

A. Procedures

Using the number of e^+e^- pairs together with the known pair production cross section on hydro-

TABLE II. Event statistics by topologies.

Topology [a]	Events found in scan: Exposures 1, 2	Exposures 3, 4	All	No fits	Not "well measured" [b]
1-prong [c]	696	...	696	...	...
3-prong [d]	10478	10380	20858	72	1171
5-prong	5235	5091	10326	50	824
7-prong	1019	1029	2048	12	197
9-prong	94	78	172	0	28
With visible strange-particle decay	1056	1535	3041	50	264
Sum	19028	18113	37141	184	2484
Pairs counted	46045	31695	77740		
Frames for count	8516	5523	14039		
Good frames	622164	578630	1200794		

[a] An N-prong event has N outgoing charged particles without detected strange-particle decay.
[b] Remeasurable events and events which are unmeasured due to secondary interaction.
[c] From 140000 pictures.
[d] Includes events with unseen recoil proton.

gen (σ_{pair}), we obtain hadronic cross sections from

$$\sigma(\gamma p \to \text{hadrons}) = \frac{N_{\text{events}}}{N_{\text{pairs}}}\,\sigma_{\text{pair}} .$$

We use the pair cross sections calculated by Knasel,[5] which are tabulated in Ref. 5 and in Table III of Ref. 1.

For cross-section calculations, a fiducial-volume cut, an energy cut, and a scanning correction were applied in this order to the number of events and pairs found in the scan. These corrections are given in Table III as fractions of the event numbers for each topology. In the following paragraphs we discuss these corrections in more detail.

To exclude events and pairs produced by nonbeam photons, the vertices of events and pairs used for the final analysis are required to be within the fiducial volume. It is defined by a cylinder along the beam direction y given by

$$R = \left[[x - x_0(y)]^2 + \left(\frac{z - z_0(y)}{2} \right)^2 \right]^{1/2} < 2 \text{ mm} ,$$

where $x_0(y)$ and $z_0(y)$ were obtained from a straight-line fit to the vertex position of the events; (x,y,z) is the vertex position of the individual event or pair. The fraction of pairs with $E_\gamma > 0.5$ GeV outside the fiducial volume was calculated from the vertex distribution of events fitting $\gamma p \to p\pi^+\pi^-$ using the known pair and event cross sections.

The photon energy spectrum, for $E_\gamma > 0.5$ GeV, was calculated from the E_γ distribution of events with $R < 2$ mm, which fit $\gamma p \to p\pi^+\pi^-$. We used the known cross sections for this channel[1,6,7] and assumed that the cross section is constant in the energy region 8–10.3 GeV. For $E_\gamma < 0.5$ GeV we used pairs to determine the photon spectrum (see Ref. 1). The resulting photon spectrum is shown in Fig. 1.

The numbers of events and pairs produced by photons outside the interval 8–10.3 GeV were calculated from the photon spectrum of Fig. 1 and from the known topology[1] and pair cross sections. The flux for all exposures, after the fiducial volume and energy cuts, yields 289 ± 6 events/μb.

The scanning corrections were determined from a quadruple scan of 10% of the film. The resulting corrections are 6%, 0.7%, and 0.09% for events with one, three, and five charged particles, respectively. Additional corrections for undetected events with a very short proton track (with momentum transfer squared to the proton $|t| < 0.02$

TABLE III. Corrections in percent to be applied to events of exposures 1, 2 (first column of Table II) in order to obtain topological cross sections.

Correction \ Topology	1-prong	3-prong	5-prong	7-prong	9-prong	With strange particle decay	Pairs
Fiducial cut	−37 ± 2	−3 ± 0.3	−1 ± 0.2	−0.7 ± 0.7	−2 ± 2	−1 ± 0.4	−3.3 ± 0.7
Energy cut	−41 ± 5	−7 ± 0.7	−3 ± 0.5	−1.5 ± 0.5	...	−4 ± 0.7	−8.1 ± 0.7
Scanning correction	+6 ± 3	+2 ± 0.7	+0.1 ± 0.1	...	...	+1.3 ± 0.6	0 ± 1

GeV^2) are 6%, 3.9%, and 2.1% for the channels $p\pi^+\pi^-$, pK^+K^-, and $p\pi^+\pi^-\pi^0$, respectively.[8] The correction was determined by an extrapolation of the measured t distribution for $|t|>0.02$ GeV^2, fitted to the form e^{At}, with A depending on $M_{\pi^+\pi^-}$ or $M_{\pi^+\pi^-\pi^0}$. The contamination of the 3-prong sample by wide-angle e^+e^- pairs was calculated by a Monte Carlo program and was found to be negligible (0.1 μb for $|t|>0.02$ GeV^2).

Electrons from identified Dalitz pairs were not counted as hadronic tracks. We calculate that $(70\pm20)\%$ of the expected Dalitz pairs were identified at the scan table. Thus cross-section corrections for unidentified Dalitz pairs were generally $\lesssim 2\%$ and were therefore not applied.

Finally, we have to discuss two corrections which are relevant only for the calculation of channel cross sections.

In the kinematic fitting to the channel hypotheses listed in Sec. I, we required the relative momentum error for each track to be smaller than 20%, unless the momentum error itself was smaller than 50 MeV/c, or the dip of the track was bigger than 0.7 rad. The numbers of events not passing this test are listed by topology in Table II. About three-fourths of these are unmeasurable because of secondary interactions close to the primary vertex. The rest did not get a satisfactory measurement. All channel cross sections in each topology were corrected by the fractions of "not well measured" events.

A small fraction ($\leq 0.5\%$) of the events gave no kinematically acceptable fits (see column "No fits" in Table II). These were ascribed to hypotheses with unobserved strange particle decay.

B. Total and Topological Cross Sections

We used the first two exposures to determine total and topological cross sections. The cross sections were calculated by applying the corrections of Table III to the numbers given in the first column of Table II. The 1-prong cross section is based on 140 000 pictures. Results are given in Table IV.

C. Channel Cross Sections

In this section we calculate the cross sections for the channels leading to three-constraint (3C) fits (no neutral particles in the final state) and zero-constraint (0C) fits (one neutral particle in the final state). The channels studied are listed in Table V.

The channel cross sections were determined using all exposures, after applying the cuts and corrections described in Sec. IIIA.

1. 3C Channels

For the reactions

$$\gamma p \to p + m\pi^+ + m\pi^-, \quad m = 1, 2, 3, 4 \tag{1a}$$

$$\gamma p \to p + K^+ + K^- + l\pi^+ + l\pi^-, \quad l = 0, 1, 2, \tag{1b}$$

$$\gamma p \to 2p + \bar{p}, \tag{1c}$$

only the beam energy is unknown. The events were selected by requiring a three-constraint (3C) kinematic fit with $\chi^2 < 30$ and consistency with the observed ionization. The fitted photon energy was required to lie within the interval 8–10.3 GeV. All alternative 0C fits were disregarded.

The contamination of the sample by events with neutral particles in the final state, giving an acceptable 3C fit, was studied with the measurement simulation program PHONY.[9] It was found to be negligible for the 3-prong events. In the 5- and 7-prong topologies 0.5% of the generated $p2\pi^+2\pi^-\pi^0$ events and 1.5% of the generated $p3\pi^+3\pi^-\pi^0$ events gave fits to reaction (1a) [but not to (1b)]. Generated $n3\pi^+2\pi^-$ and $n4\pi^+3\pi^-$ events yielded negligible fractions of such fits. These estimated contaminations were subtracted from the 3C samples. Considering next the unique events of reaction (1b), we removed the contamination due to 0C events by imposing a $\chi^2 < 8$ cut. This follows from the observation that all fits to reaction (1b) of the generated 0C events had a $\chi^2 > 8$.

For the events that were ambiguous between (1a) and (1b) the 0C contamination was removed by excluding those events which had fits to both reactions with $\chi^2 > 7$. The numbers of events obtained after subtracting the 0C contamination are given in Table V. The remaining ambiguities were assigned by choosing the hypothesis with the smaller χ^2. The systematic uncertainties of this procedure are included in the errors. The cleanness of all samples [reactions (1a)–(1c)] was

TABLE IV. Topological and total cross section in the energy interval $8 \leq E_\gamma \leq 10.3$ GeV.

Topology	σ (μb)
1-prong	8.5 ± 1.1
3-prong[a]	64.1 ± 1.5
5-prong	34.2 ± 0.9
7-prong	6.8 ± 0.3
9-prong	0.61 ± 0.08
With visible strange particle decay	9.8 ± 0.4
Total cross section	124.0 ± 2.5

[a] Includes 2-prong topology.

TABLE V. Channel event numbers and cross sections.

Channel	Constraints	No. of events [a] Unique	Ambiguous	All	Cross section (μb)
			I. 3-prong		
$p\pi^+\pi^-$	3C	3742 ± 61	9 ± 5	3751 ± 61	14.7 ± 0.6
pK^+K^-	3C	148 ± 12	5 ± 5	153 ± 13	0.58 ± 0.05 [b]
$2p\bar{p}$	3C	25 ± 5	···	25 ± 5	0.09 ± 0.02
$p\pi^+\pi^-\pi^0$	0C	1886 ± 143	203 ± 166	2089 ± 219	7.5 ± 0.8
$n2\pi^+\pi^-$	0C	63 ± 51	845 ± 191	908 ± 198	3.2 ± 0.7
Multineutral					38.0 ± 1.9
			II. 5-prong		
$p2\pi^+2\pi^-$	3C	1035 ± 32	44 ± 13	1079 ± 35	4.1 ± 0.2
$pK^+K^-\pi^+\pi^-$	3C	108 ± 13	13 ± 13	121 ± 21	0.46 ± 0.08 [b]
$p2\pi^+2\pi^-\pi^0$	0C	1526 ± 130	334 ± 236	1860 ± 269	6.7 ± 1.0
$n3\pi^+2\pi^-$	0C	32 ± 32	464 ± 278	496 ± 280	1.8 ± 1.0
Multineutral					21.1 ± 1.7
			III. 7-prong		
$p3\pi^+3\pi^-$	3C	222 ± 16	6 ± 5	228 ± 17	0.87 ± 0.06
$pK^+K^-2\pi^+2\pi^-$	3C	10 ± 3	5 ± 5	15 ± 6	0.06 ± 0.02 [b]
$p3\pi^+3\pi^-\pi^0$	0C	362 ± 60	109 ± 96	471 ± 113	1.7 ± 0.4
$n4\pi^+3\pi^-$	0C	10 ± 10	237 ± 102	247 ± 102	0.9 ± 0.4
Multineutral					3.3 ± 0.6
			IV. 9-prong		
$p4\pi^+4\pi^-$	3C	20 ± 5	···	20 ± 5	0.08 ± 0.02
$p4\pi^+4\pi^-\pi^0$	0C	54 ± 7	8 ± 3	62 ± 8	0.25 ± 0.03
$n5\pi^+4\pi^-$	0C	8 ± 8	17 ± 4	25 ± 9	0.10 ± 0.03
Multineutral					0.18 ± 0.09

[a] See text for error estimation.
[b] Events with visible K decay are included in the cross-section calculation.

checked by plotting the χ^2 and E_γ distributions (not shown) which were consistent with those expected for genuine 3C events.

2. 0C Channels

We next turn to the channels

$$\left.\begin{aligned}\gamma p &\to p + m\pi^+ + m\pi^- + \pi^0 \\ \gamma p &\to n + (m+1)\,\pi^+ + m\pi^-\end{aligned}\right\} \quad m = 1, 2, 3, 4\ . \qquad \begin{matrix}\text{(2a)}\\ \text{(2b)}\end{matrix}$$

All events which did not get an accepted 3C fit were "fitted" to hypotheses (2a) and (2b). These fits originate from genuine events of channels (2a) or (2b) and from events of the corresponding multineutral channels

$$\gamma p \to p + m\pi^+ + m\pi^- (+\text{neutrals}), \qquad \text{(2c)}$$

$$\gamma p \to n + (m+1)\,\pi^+ + m\pi^- (+\text{neutral(s)}). \qquad \text{(2d)}$$

The separation of the channels was based on distributions of the missing mass squared $(\text{MM})^2$, calculated from the measured track quantities and the average photon energy of each exposure. No energy cut was applied. However, the separation method made use of the program PHONY,[9] which generated simulated events with the observed energy spectrum for $5 < E_\gamma < 10.3$ GeV. Therefore the flux for computing the 0C cross sections was calculated with an energy cut at 5 GeV. The corresponding cross section equivalent is 302 ± 6 events/μb.

In the following we discuss first the samples which have a unique fit to either hypothesis (2a) or (2b), i.e., either a proton was identified or all tracks were identified as pions, and then discuss the ambiguous events. In processing the PHONY[9] generated samples, events of reaction (2a) with proton tracks of momentum < 1.5 GeV and of reaction (2b) with all pion tracks of momentum < 1.5 GeV were considered unique. The others were considered ambiguous.

(a) Unique Events of Channel $\gamma p \to p + m\pi^+ + m\pi^- + \pi^0$

Figure 2 shows the distribution of $(\text{MM})^2$ for the unique sample in the different topologies. The π^0 signal around 0.02 GeV^2 is clearly visible. We have followed two approaches to extract the number of events in channel (2a).

Method 1. We performed in each topology a χ^2 fit of the experimental $(MM)^2$ distributions in Fig. 2, in the region $-0.5<(MM)^2<1.5$ GeV^2, to the sum of the following four contributions:

(i) The shape of the $(MM)^2$ distribution for unique events of channel (2a) as estimated by PHONY[9] generation of the following channels (weighted with the t distributions in parentheses) $p\rho^0\pi^0(e^{4t})$, $p\pi^+\pi^-\pi^0(e^t)$, $p2\pi^+2\pi^-\pi^0(e^{4t}, e^t)$, and $p3\pi^+3\pi^-\pi^0(e^t)$.

The generated $(MM)^2$ distributions become narrower, the steeper the t distribution and the higher-multiplicity the topology. We used for each topology the average of the distributions of the corresponding generated channels.

(ii) The $(MM)^2$ distribution of the PHONY[9] generated $p\omega(e^{7t})$ channel which was much narrower

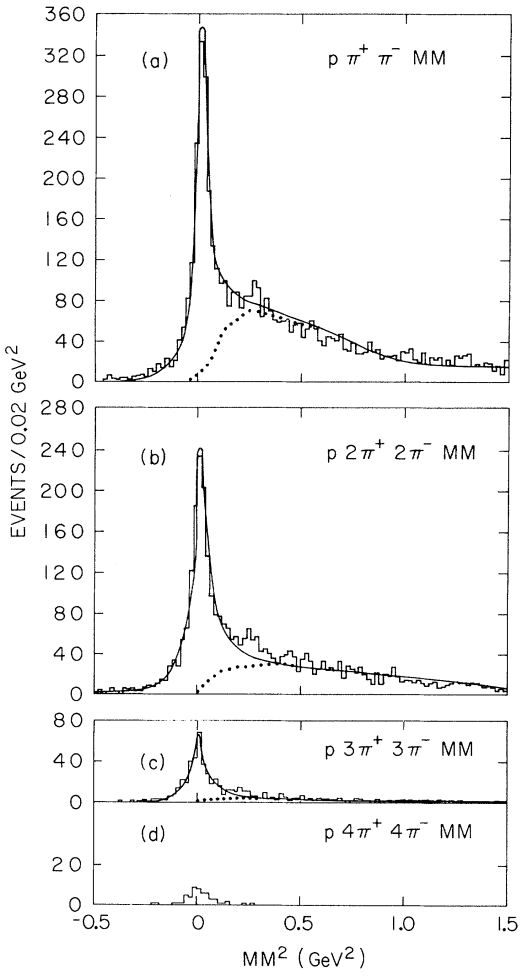

FIG. 2. $(MM)^2$ distributions for unique fits to hypothesis (2a). The solid lines are the results of the χ^2 fit to single π^0 and multineutral background distributions. The dotted lines represent the multineutral background alone.

TABLE VI. Estimated number of events in the channel $\gamma p \to p + m\pi^+ + m\pi^- + \pi^0$ with unique fits.

Method	3-prong	5-prong	7-prong
1. Fit	1886 ± 143	1526 ± 130	362 ± 30
2. "Symmetrization" of $(MM)^2 < 0.02$ GeV^2 events	1893 ± 71	1511 ± 61	429 ± 30

than the rest. It was taken as representative of possibly other resonance channels with the same characteristic which were not generated, and was fitted as an independent contribution in all topologies.

(iii) The multineutral background representing the sum of the various $(MM)^2$ distributions from channels with two or more neutrals [channels (2c)]. The shapes of these distributions were derived by using the events in the higher-multiplicity topologies with proton momentum <1.5 GeV/c. A $\pi^0\pi^0$ pair was substituted for every possible $\pi^+\pi^-$ pair and $(MM)^2$ was recalculated. The relative weight of each multineutral channel was derived by a simple isospin model[10,11] from event numbers in the corresponding all-charged or single-neutral channels. A more detailed description of the procedure is given in Refs. 1 and 3.

(iv) Two additional contributions in the 3-prong topology: one from $\eta \to$ neutrals estimated from the $\eta \to \pi^+\pi^-\pi^0$ decay signal in the $p2\pi^+2\pi^-\pi^0$ channel, and the other from the channel $pB^0 \to p\omega\pi^0 \to p\pi^+\pi^-\pi^0\pi^0$ which was observed at 2.8 and 4.7 GeV (Ref. 3) and which occurs at 9.3 GeV with a cross section of about 1 μb. These resonance contributions are not specifically taken into account by our general background construction and were added with their absolute normalizations.

The free parameters of the first series of fits were the normalizations of contributions (i)–(iii) above. The amounts of the "$p\omega$" contribution required by the fit were 39%, 26%, and 0% of the fitted total number of events of reaction (2a) in the 3-, 5-, and 7-prong topologies, respectively. We performed a second series of fits with the observed[12] amount of $p\omega$ (25%) in the 3-prongs, and without this component in the 5-prongs, and obtained results within one standard deviation of the previous ones, while the χ^2 of the fits increased. For the multineutral background, normalizations of 1.2–1.4 relative to the absolute prediction of the model[10] were required.

The results of the first series of fits are given in Table VI and the fitted distributions are shown in Fig. 2. A good over-all description of the experimental distributions is apparent, except in the 5-prong channel which has an excess of events in

the region $0.2 < (\mathrm{MM})^2 < 0.4$ GeV^2, which are not accounted for by our background.

Method 2. We make use of the fact, demonstrated in Fig. 2, that there is very little background below $M_{\pi^0}{}^2$. The fraction of events of channel (2a) below $(\mathrm{MM})^2 = 0.02$ GeV^2 can be estimated from the PHONY[9] generated events. This fraction does not show any strong systematic variation with topology, t region, or resonance channel generated, and seems to be a general property connected to the shape of the photon energy spectrum. The average fraction is $(53.4 \pm 1.1)\%$. We thus used it to compute the number of unique events of channel (2a) from the experimental number of events with $(\mathrm{MM})^2 < 0.02$ GeV^2 (after subtracting the small multineutral background.)

This method depends very little on the shape of the multineutral background and, as such, serves as a useful check on the results of the first method. And indeed, we see from Table VI that the results of the two methods agree well. The numbers derived by the first method are entered in Table V and were used for the cross-section calculation. For the 7-prongs, the fit error was doubled to cover the result of Method II.

(b) *Unique Events of Channel* $\gamma p \to n + (m+1)\,\pi^+ + m\pi^-$

At 9.3 GeV fewer than 10% of the neutron events are unique. As shown in Fig. 3 the $(\mathrm{MM})^2$ distributions of these unique events are quite flat. The multineutral background was calculated using the isospin model described in the previous section. No over-all normalization of the multineutral background was necessary. To obtain the number of single-neutral events the background was subtracted for $(\mathrm{MM})^2 < 1.25$ GeV^2. The error was taken as the amount of background subtracted. The numbers obtained are listed in Table V.

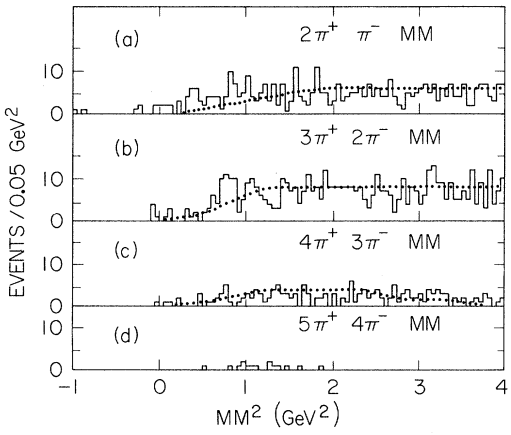

FIG. 3. $(\mathrm{MM})^2$ distributions for unique fits to hypothesis (2b). The dotted lines represent the multineutral background.

(c) *Ambiguous Events*

We now try to separate events from channels (2a) and (2b) which lead to ambiguous fits. The ambiguous sample presents special problems. Some fits of hypothesis (2a) are ambiguous among themselves (i.e., with fits in which p and π^+ are permuted). In addition, the π^0 and neutron peaks in the $(\mathrm{MM})^2$ distribution are broad and superimposed on a strong multineutral background and a reflection from events of the other channel.

The experimental $(\mathrm{MM})^2$ distributions are shown in Figs. 4 and 5. Figure 4 includes all fits to hypothesis (2a) (the events with self-ambiguous fits appear several times). In each topology we made a simultaneous χ^2 fit to the $(\mathrm{MM})^2$ distribution of Fig. 4, in the range $-0.5 < (\mathrm{MM})^2 < 1.5$ GeV^2, and to the $(\mathrm{MM})^2$ distribution of Fig. 5, in the range $-0.5 < (\mathrm{MM})^2 < 4.0$ GeV^2, using the contributions (i)–(iii) below:

(i) The two $(\mathrm{MM})^2$ distributions from PHONY[9] generated ambiguous events of channels (2a) and (2b). (The latter generated with an e^{4t} distribution.)

(ii) From the same PHONY[9] events we obtained the reflection of one channel into the $(\mathrm{MM})^2$ distribution of the other channel.

(iii) The multineutral background was calculated from events of higher multiplicity with proton momentum in channel (2a) or at least one π^+ momentum in channel (2b) > 1.5 GeV. All proton events were also interpreted as neutron events and reflected into the neutron channel and vice versa. The relative weights of the different multineutral channels were derived from the isospin model.[10]

The parameters of the fit were the numbers of ambiguous events to be assigned to channels (2a) or (2b), as well as the two independent normalizations of the multineutral backgrounds for the two $(\mathrm{MM})^2$ distributions. The fitted assignments of ambiguous events are given in Table V. The background normalization factors came out between 1 and 2 times the prediction of Ref. 10. The curves in Figs. 4 and 5 show the fitted $(\mathrm{MM})^2$ distributions for the 3-, 5-, and 7-prong fits of channels (2a) and (2b), respectively.

The $(\mathrm{MM})^2$ distributions in Figs. 4 and 5 do not show sharp π^0 and n peaks. Therefore, the results of the fits are sensitive to the shape of the input distributions of the single-neutral and multineutral events. This uncertainty is not fully represented by the fit errors because the shapes of the various contributions were kept fixed. The errors entered

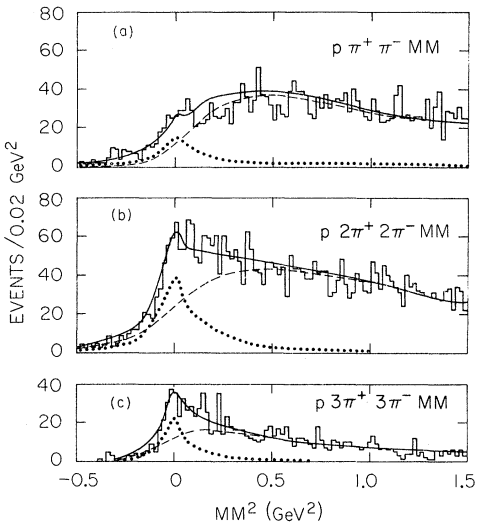

FIG. 4. $(MM)^2$ distributions for ambiguous fits to hypothesis (2a) in the different topologies. Solid lines are the results of the χ^2 fit described in the text. Dashed lines represent the fitted multineutral background and reflection of channel (2b). Dotted lines represent the fitted contribution of channel (2a).

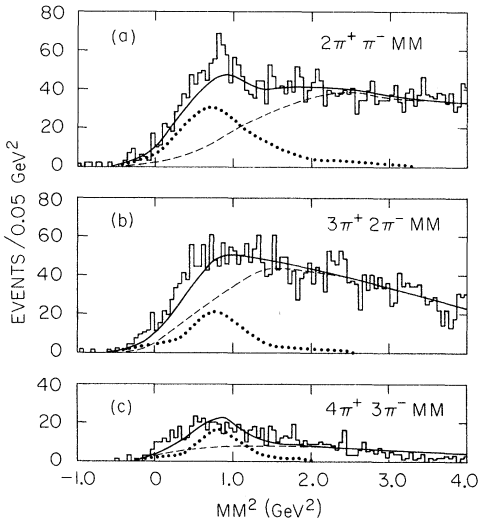

FIG. 5. $(MM)^2$ distribution for ambiguous fits to hypothesis (2b) in the different topologies. Solid lines are the results of the χ^2 fit described in the text. Dashed lines represent the fitted multineutral background, and reflection of channel (2a). Dotted lines represent the fitted contribution of channel (2b).

in Table V were computed therefore in the following way: The upper limit on the event number in channel (2a) was estimated by Method II of section (a), assuming no reflection from channel (2b) for $(MM)^2 < 0.02$ GeV^2. The simultaneous fits were then repeated, fixing channel (2a) at this limit, and the number of events in channel (2b) was determined; this was used as the lower limit for channel (2b).

As the reflection of channel (2a) on (2b) peaks around M_n^2, the procedure is not feasible for estimating an upper (lower) limit for channel (2b) [(2a)], and therefore the limits were symmetrized.

The 9-prong events were individually assigned to (2a) or (2b) by selecting that interpretation which gave a $(MM)^2$ closer to the $M_{\pi^0}^2$ or M_n^2.

3. *Multineutral Channels*

In contrast to the situation at 4.7 GeV,[1] at 9.3 GeV most of the multineutral events from channels (2c),(2d) are ambiguous. Their separation is not possible without model assumptions. We therefore give only the cross sections for the sum of both channels in Table V.

IV. RESULTS AND DISCUSSION

The total and topological cross sections (Sec. III B) are displayed in Table IV and Fig. 6. Our total cross section is in agreement with measurements of Hesse *et al.*[13] For comparison, the lower-energy results[1] are also shown in Fig. 6.

The channel cross sections are given in Table V and shown in Figs. 7–9. To present the energy dependence of the cross sections, we also show results from previous experiments.[1,6,7]

The cross section for $\gamma p \to p\pi^+\pi^-$ (Fig. 7) has a prominent maximum around 0.7–1 GeV and then levels off to a value of about 15 μb at 10 GeV. The maximum is due to strong $\Delta^{++}\pi^-$ production.[6] An

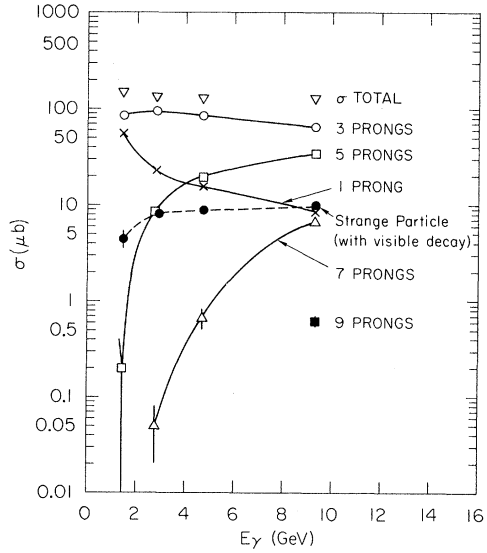

FIG. 6. Total and topological photoproduction cross sections from this experiment (lower-energy results from Ref. 1) versus incoming photon energy. The lines are provided only to help distinguish between topologies.

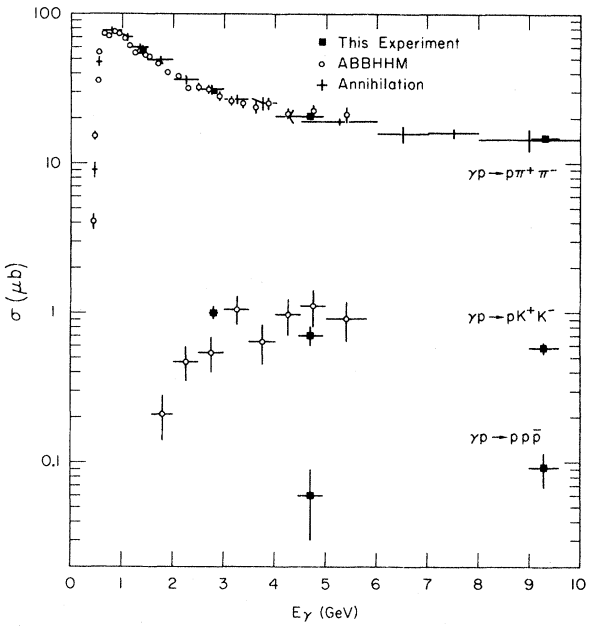

FIG. 7. Three-body cross sections, from this experiment (lower-energy results from Ref. 1), from the ABBHHM collaboration (Ref. 6) and from the annihilation experiment (Ref. 7), versus incoming photon energy.

equivalent maximum does not occur in $\gamma p \to pK^+K^-$. Above 3 GeV the $p\pi^+\pi^-$ and pK^+K^- cross sections have a comparable energy dependence. At 9.3 GeV about 90% (50%) of the channel $p\pi^+\pi^-$ (pK^+K^-) proceeds via ρ^0 (ϕ) production.[12] The ratio of $\pi^+\pi^-$, K^+K^-, and $p\bar{p}$ pair production is 160:6.4:1 at 9.3 GeV. From Figs. 8 and 9 we note that cross sections for channels with the same number of mesons have a similar energy dependence.

We can compare the following cross-section

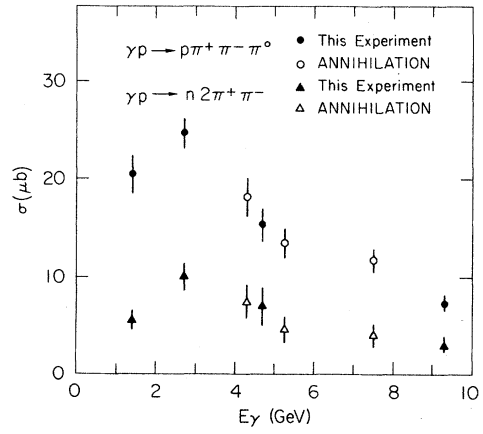

FIG. 8. Four-body cross sections, from this experiment (lower-energy results from Ref. 1) and from the annihilation experiment (Ref. 7), versus incoming photon energy.

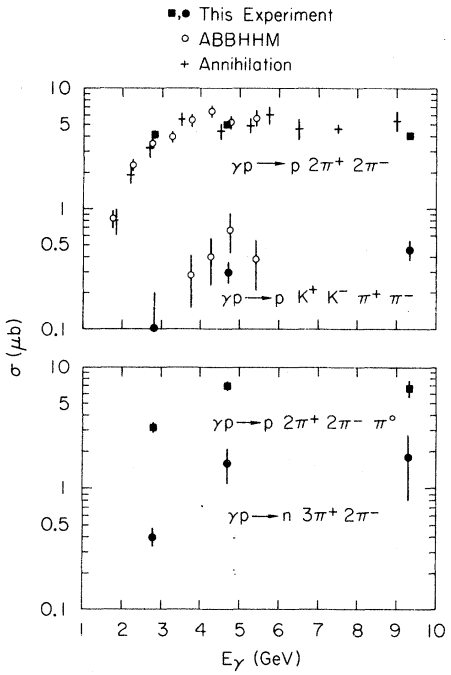

FIG. 9. Five- and six-body cross sections, from this experiment (lower-energy results from Ref. 1), from the ABBHHM collaboration (Ref. 6) and from the annihilation experiment (Ref. 7), versus incoming photon energy.

ratios to the predictions of the statistical model mentioned in Sec. III C 2[10,11]:

$$R_3 = \frac{\sigma(\gamma p \to p\pi^+\pi^-\pi^0)}{\sigma(\gamma p \to n2\pi^+\pi^-)},$$

$$R_5 = \frac{\sigma(\gamma p \to p2\pi^+2\pi^-\pi^0)}{\sigma(\gamma p \to n3\pi^+2\pi^-)},$$

$$R_7 = \frac{\sigma(\gamma p \to p3\pi^+3\pi^-\pi^0)}{\sigma(\gamma p \to n4\pi^+3\pi^-)}.$$

The model implies a statistical distribution of particle charges for final states with fixed particle numbers, on the basis of isospin invariance. It predicts $R_3 = 1.8$, $R_5 = 2.7$, and $R_7 = 3.65$. Experimentally, we find at 9.3(4.7) GeV $R_3 = 2.3 \pm 0.6$ (2.1 ± 0.6), $R_5 = 3.7 \pm 2.2$ (4.4 ± 0.9), and $R_7 = 1.9 \pm 1$ (4.3 ± 2.6), in reasonable agreement with the statistical model.

ACKNOWLEDGMENTS

We wish to thank the SLAC Operations Crew, R. Watt, and the 82-in. Bubble Chamber Operations Group for their assistance in performing this experiment. We acknowledge the diligence of our scanners and data reduction group, in particular D. Blohm, K. Eymann, W. Hendricks, and A. Wang.

*Work supported by the U.S. Atomic Energy Commission and National Science Foundation.
†Present address: University of Washington, Seattle, Wash.
‡Present address: University of Massachusetts, Amherst, Mass.
§Present address: DPHPE, CEN, Saclay, France.
||Present address: Weizmann Institute, Rehovoth, Israel.
**Present address: Max-Planck-Institut für Physik und Astrophysik, München, Germany.
††Present address: University of Glasgow, Physics Department, Glasgow, Scotland.
‡‡Present address: University of Hamburg, Hamburg, Germany.
§§Present address: DESY, Hamburg, Germany.
[1]J. Ballam *et al.*, Phys. Rev. D **5**, 545 (1972).
[2]C. K. Sinclair *et al.*, IEEE Trans. Nucl. Sci. **16**, 1065 (1969).
[3]W. J. Podolsky, Ph.D. thesis, LBL Report No. UCRL-20128, 1971 (unpublished).
[4]R. H. Milburn, Phys. Rev. Lett. **10**, 75 (1963); J. J. Murray and P. R. Klein, SLAC Report No. SLAC-TN-67-19, 1967 (unpublished).
[5]T. M. Knasel, DESY Report No. 70/3, 1970 (unpublished).
[6]Aachen-Berlin-Bonn-Hamburg-Heidelberg-München Collaboration, Phys. Rev. **175**, 1669 (1968); Phys. Rev. **188**, 2060 (1969); H. Spitzer, DESY Internal Report No. DESY-Fl 71/4, 1971 (unpublished).
[7]Y. Eisenberg *et al.*, Phys. Rev. D **5**, 15 (1972).
[8]In the channel $\gamma p \to p\pi^+\pi^-$ about half the "missing" events were found in the scan as 2 prongs, with unseen recoil proton.
[9]E. Burns and D. Drijard, PHONY , Trilling-Goldhaber Group Technical Note 143, Lawrence Radiation Laboratory, Berkeley, 1968 (unpublished).
[10]H. Spitzer, Ph.D. thesis, Hamburg, DESY Internal Report No. DESY Fl/4, 1967 (unpublished).
[11]J. Shapiro, Nuovo Cimento Suppl. **18**, 40 (1960).
[12]J. Ballam *et al.*, Phys. Rev. D **7**, 3150 (1973).
[13]W. P. Hesse *et al.*, Phys. Rev. Lett. **25**, 613 (1970).

PHYSICAL REVIEW D VOLUME 8, NUMBER 5 1 SEPTEMBER 1973

New Experimental Results on $\bar{p}p \to K^0\bar{K}^0$ from 700 to 1100 MeV/c *

R. R. Burns, P. E. Condon, J. Donahue, M. Mandelkern, L. R. Price, and J. Schultz
Department of Physics, University of California, Irvine, California 92664
(Received 23 August 1972)

Cross sections and angular data are presented for proton-antiproton annihilation into K_SK_L and K_SK_S at six laboratory momenta from 686 to 1098 MeV/c. Unlike results reported elsewhere, the rates for $C=-1$ and $C=+1$ states are found to be comparable within statistics. Also, evidence is presented that at least several waves contribute to the direct-channel amplitude with different isospin as well as angular momentum quantum numbers.

Recently, Benvenuti *et al.*[1] reported that in the final state $\bar{p}p \to K^0\bar{K}^0$ they found only one event of the type

$$\bar{p}p \to K_SK_S, \tag{1}$$

while in the same film they found 71 events of the type

$$\bar{p}p \to K_S(K^0), \tag{2}$$

where K_S represents a visible $K_S^0 \to \pi^+\pi^-$ and (K^0) represents an unobserved K^0 meson. They found an enhancement in reaction (2) at a beam momentum of about 600 MeV/c. (Most of their data were in the 400–800-MeV/c range.) Based on the near absence of reaction (1) they concluded that this effect must have $C=-1$. From their angular analysis they also concluded that this effect probably has $J=1$, and proposed the name $\rho(1970)$ for this state.[2]

Our experiment (performed in the same beam and hydrogen bubble chamber) covers $\bar{p}$ initial momentum from 700 to 1100 MeV/c, thus overlapping about 20% of the data of Benvenuti *et al.* Since our data do not extend down to 600 MeV/c, we cannot comment on the existence of their enhancement. However, we observe a significant rate for reaction (1). In fact, we find the cross sections for reactions (1) and (2) roughly equal over our entire energy range. As regards the region of overlap, this result is in disagreement with the observation of Benvenuti *et al.*, and we believe that it may cast some doubt on their assertion that their effect must be pure $C=-1$.

Our data were taken from 220 000 photographs of antiproton interactions in the BNL 30-inch hydrogen bubble chamber. The chamber was exposed to the AGS antiproton beam at the six mean lab momenta of 686, 772, 861, 943, 1037, and 1098 MeV/c.

The film was scanned and measured twice for events having one or more V' s pointing back to a zero-pronged vertex. Approximately 575 events were found and measured. The combined scanning efficiency was $(82\pm3)\%$, with no significant variation with beam momentum.

The events were processed by the programs TVGP-SQUAW . Eight events were observed to fit $\bar{p}p \to K_SK_S$, with confidence levels greater than 1% for a ten-constraint fit. Thirty-five events were observed to fit $\bar{p}p \to K_S(K^0)$, with confidence